Engineering Fracture Mechanics 75 (2008) 4019–4035

Contents lists available at ScienceDirect

Engineering Fracture Mechanics

journal homepage: www.elsevier.com/locate/engfracmech

Effects of repeated loading on the fracture behavior of notched TiAl specimens

R. Cao [a], J.H. Chen [a,*], J. Zhang [b], H. Zhu [a]

[a] State Key Laboratory of Advanced Non-ferrous Metal Materials, Lanzhou University of Technology, Lanzhou, Gansu 730050, PR China
[b] High Temperature Material Research Division, Central Iron and Steel Research Institute, Beijing 100081, PR China

ARTICLE INFO

Article history:
Received 19 December 2006
Received in revised form 15 March 2008
Accepted 26 March 2008
Available online 8 April 2008

Keywords:
TiAl alloy
In situ tensile test
Notched specimen
Microcracks

ABSTRACT

Notched specimens of a fully lamellar TiAl alloy and a duplex TiAl alloy were in situ tensile tested with repeated loading–unloading–reloading processes in a scanning electron microscope (SEM). The step-by-step processes of initiation and extension of the main crack were captured by SEM. The fracture surfaces were observed and one-sector-to-one-sector related to the crack extension. Effects of loading–unloading damage on the fracture behavior were evaluated by combining the pictures of propagating crack configurations, corresponding fracture surfaces and the load locus. The results revealed the following events: (1) at the elastic regime, the loading–unloading process had negligible effect on the fracture behavior produced by subsequent reloading; (2) at the plastic regime, even at a value much lower than that of the preload, the reload extended further the existing main crack; (3) after a heavy loading–unloading process, the main crack extended and resulted in final fracture at a value of the reload, which was lower than that of the preload and (4) microcracks produced in the loading–unloading process had minor effects on the fracture behavior.

1. Introduction

Many works have been published regarding the formation of a diffuse zone of microcracks and ligaments between cracks ahead of a crack-tip as a mechanism to improve toughness [1–6]. Zheng et al. [7] investigated the effects of microcracks on the plastic deformation of a fully lamellar (FL) γ-TiAl alloy. They concluded that fracture load decreased with increasing microcrack density. The larger the grain size, the higher the microcrack density, thus, the higher the apparent plasticity and the lower the fracture stress.

In Ref. [8], Bartels et al investigated the strain rate-dependence of the deformation mechanisms in a FL γ-TiAl alloy and concluded: The cracking behavior depended on the strain rate. At a strain rate of $5 \times 10^{-3}\ s^{-1}$ (quasi-static conditions), the FL samples showed large cracks in the direction of the compression cone, whereas dynamically compressed specimens ($2–4 \times 10^{3}\ s^{-1}$) exhibited great number of shorter interlamellar microcracks. Obviously, the high strain rate increased the crack initiation rate and diminished the crack propagation.

In Ref. [9], Zhou et al indicated that the tensile strength and the strain to fracture increased with increasing strain rate.

In the authors' previous work [10], effects of load–unload-induced microcrack damage on fracture behavior were investigated in flat specimens by tensile tests. It concluded that: (a) microcracks produced through the entire specimen volume decreased the apparent elastic modulus and resulted in a descendant sector of the load–displacement curve just before final

* Corresponding author. Present address: President Office, Lanzhou University of Technology, Lanzhou, Gansu 730050, PR China. Tel.: +86 931 2757296; fax: +86 931 2755806.
E-mail addresses: zchen@lut.cn, caorui@lut.cn (J.H. Chen).

0013-7944/$ - see front matter © 2008 Elsevier Ltd. All rights reserved.
doi:10.1016/j.engfracmech.2008.03.015

fracture (volumetric effects), and (b) microcracks extended on the weakest cross section decreased the fracture load (facial effects).

As mentioned in a previous paper [11], the fracture behavior in a notched TiAl specimen was different from that in a smooth tensile test specimen. Although on the microscopic scale, the crack preferred to propagate through the lamellar boundary as an inter-lamellar crack, yet on the macroscopic scale, the fracture behavior in a notched bending specimen was different from that in a flat tensile specimen. While in a notched specimen, the main crack propagation was confined to a narrow strip extending in front of the notch where the normal stress is higher, in a smooth tensile test specimen, the fracture occurred in a randomly located weakest cross section where the density of microcracks was highest. Based on the results obtained in smooth tensile specimens, the present work focuses on the effects of load–unload–induced damage on the fracture behavior of notched specimens.

2. Experimental procedures

2.1. Materials and specimens

A TiAl alloy with compositions shown in Table 1 was used. All samples were cut from a forged pancake that had been deformed at 1100 °C to achieve a 70% height reduction. The samples were first treated by hot isostatic pressing in 950 °C, 120 MPa in Argon for 3 h, then encapsulated in quartz tubes and put into the furnace at pre-determined temperatures. Samples of duplex (DP) microstructure were obtained by annealing at 1250 °C for 18 h, and samples of fully lamellar (FL) microstructure were obtained by annealing at 1370 °C for 1 h. The two types of obtained microstructures, DP and FL are shown in Fig. 1. The colony size and the lamellar spacing of FL are 200 μm and 0.5 μm respectively, those of DP are 100 μm and 0.2 μm respectively. The size of equaxied gamma grains of DP is 50 μm.

The dimensions of notched specimens for *in situ* tensile tests are shown in Fig. 2. The thicknesses of the specimens shown in Fig. 2 were varied in the range of 0.20–1.1 mm, and the real values are shown in Table 2. Two types of notches were cut, which were Chevron notch (45° V notch) with 250 μm in root radius and slit notch (S notch) with parallel sides and 87.5 μm in root radius. Specimens were cut by electric-spark machining (ESM), mechanically polished and then etched in a solution of 10% HNO_3, 3% HF and 87% water.

2.2. Observation of in situ tensile tests in SEM

In situ tensile tests were performed under vacuum using loading stage mounted in a scanning electron microscope (SEM) S-520. The specimens (shown in Fig. 2) were step by step loaded-unloaded-reloaded. The loads were measured by a load cell calibrated by standard load sensor. Table 2 shows the dimensions of in situ tensile specimens and the measured fracture loads. Because the original ligament areas varied, the applied stress, σ, was defined as the quotient of applied load divided by the original area of ligament specimen by specimen. It really represented the applied load rather than the instant stress and was called the *applied load or applied stress*. The side views of crack configurations at various loading or unloading steps were imaged by SEM. Thus, the crack initiation and extension could be determined as a function of the applied loads. Intensive attention was paid to the crack extension, which was produced at a reload value lower than that of the preload.

2.3. Observations of fracture surfaces

Fracture surfaces were observed and imaged by SEM. Special attention was put on the fracture facet pictures taken along the path of surface crack extension which developed during in situ tensile tests. By measuring and designating the distances from the notch root to the sectors of surface cracks and the distance to the corresponding fracture facets, the fracture facets could be related in a one-to-one fashion to the sectors of surface crack. The high resistance to the crack propagation or the unstable extension of the main crack could be interpreted by comparing the surface crack sectors with the corresponding fracture facets.

2.4. FEM Calculations

A two dimensional FEM model with 8-node plane stress reduced integration elements (CPS8R) was established by ABAQUS code. Thirty elements were uniformly distributed around the notch root. A total 3,759 elements and 11,720 nodes were taken into account. The curves of engineering stress–strain (showing a Power-law hardening rule) obtained in Ref. [11] were calculated into true stress–true strain curves which were digitized point-by-point. The data were input into the ABAQUS

Table 1
Compositions of TiAl alloy (at %)

Ti	Al	V	Cr
Balance	47.5	2.5	1.0

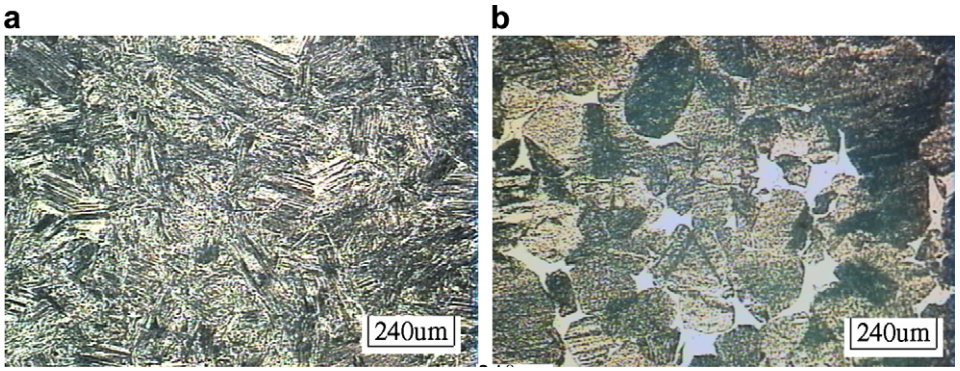

Fig. 1. Microstructures of (a) fully-lamellar and (b) duplex TiAl-based alloy.

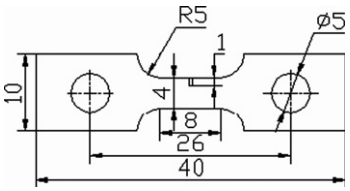

Fig. 2. Dimensions of specimens for in situ observations.

Table 2
Parameters of dimensions and measured fracture loads of in situ tensile specimens

Specimen	Ligament area (mm^2)	Thickness (mm)	Notch type	Unload process number	Notch depth (mm)	P_f (N)	σ_f (MPa)
fl-s-12	0.50 × 3	0.50	S	0	1	310.00	206.67
fl-s-4	0.30 × 3	0.30	S	1	1	130.33	144.81
fl-s-5	0.28 × 3	0.28	S	2	1	93.91	111.80
fl-s-6	0.24 × 3	0.24	S	3	1	52.00	72.23
fl-s-7	1.04 × 3	1.04	V	0	1	555.36	178.00
fl-s-9	0.36 × 3	0.36	V	1	1	128.39	118.88
fl-s-10	0.38 × 3	0.38	V	3	1	190.28	166.92
dp-s-6	0.30 × 3	0.30	S	0	1	109.53	121.70
dp-s-3	0.36 × 3	0.36	S	1	1	76.85	71.16
dp-s-5	0.24 × 3	0.24	S	2	1	69.61	96.68

Where P_f = fracture load, σ_f = fracture stress (P_f/original ligament area).

program as the materials' data. The distributions of normal stress σ_{yy} ahead of the notch root were calculated at various steps of loading–unloading–reloading procedures. Because the strains measured by tensile tests in [11] incorporated both the plastic strain and the elongation caused by microcracks and the main crack configurations could not be accurately simulated, the calculation results only offered a qualitative description.

3. Experimental results and discussions

3.1. Results and discussions of in situ tensile tests

Unlike the brittle fracture of steel at low temperature, which is triggered by an initiation of a critical crack nucleus and then unstably propagates throughout the specimen, the brittle fracture of TiAl alloy is developed by a step-by-step extension of the main crack as the applied load increased. Fig. 3a–f shows a number of "load-crack length" curves measured by in situ tensile tests of the FL TiAl alloy with various loading–unloading–reloading procedures. Fig. 4a–c show the curves for the DP TiAl alloy. The dimensions and the measured fracture loads for all in situ tensile specimens are presented in Table 2.

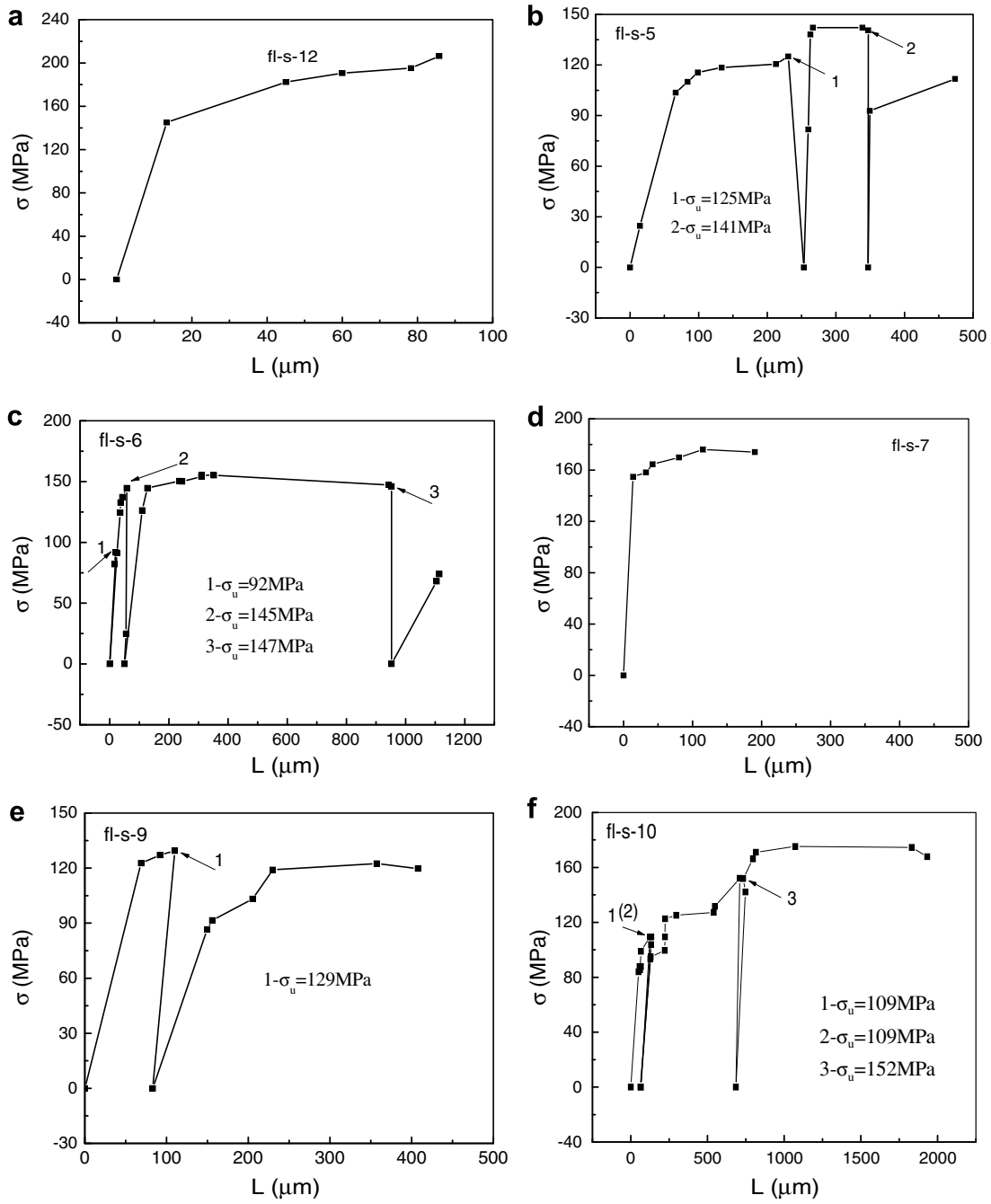

Fig. 3. Curves plotting applied stress σ against the lengths of main cracks L of fully lamellar TiAl alloys (a) fl-s-12, (b) fl-s-5, (c) fl-s-6, (d) fl-s-7, (e) fl-s-9 and (f) fl-s-10.

Table 3a–c shows the applied stresses (σ) and the corresponding crack lengths (L) recorded in in situ tests for three specimens.

From Figs. 3, 4 and Table 3, the following ideas can be drawn:

(1) When the preload was applied with the elastic regime, such as 92 MPa for specimen fl-s-6 (See Fig. 3c) after completely unloading, the main crack of 30 μm in length was fully closed. During the reloading process, the main crack opened again and extended to a length of 25 μm at 91 MPa of the applied reload. The locus of reloading against the crack length overlapped the locus of preloading. There was no extra extension of the main crack until the value of

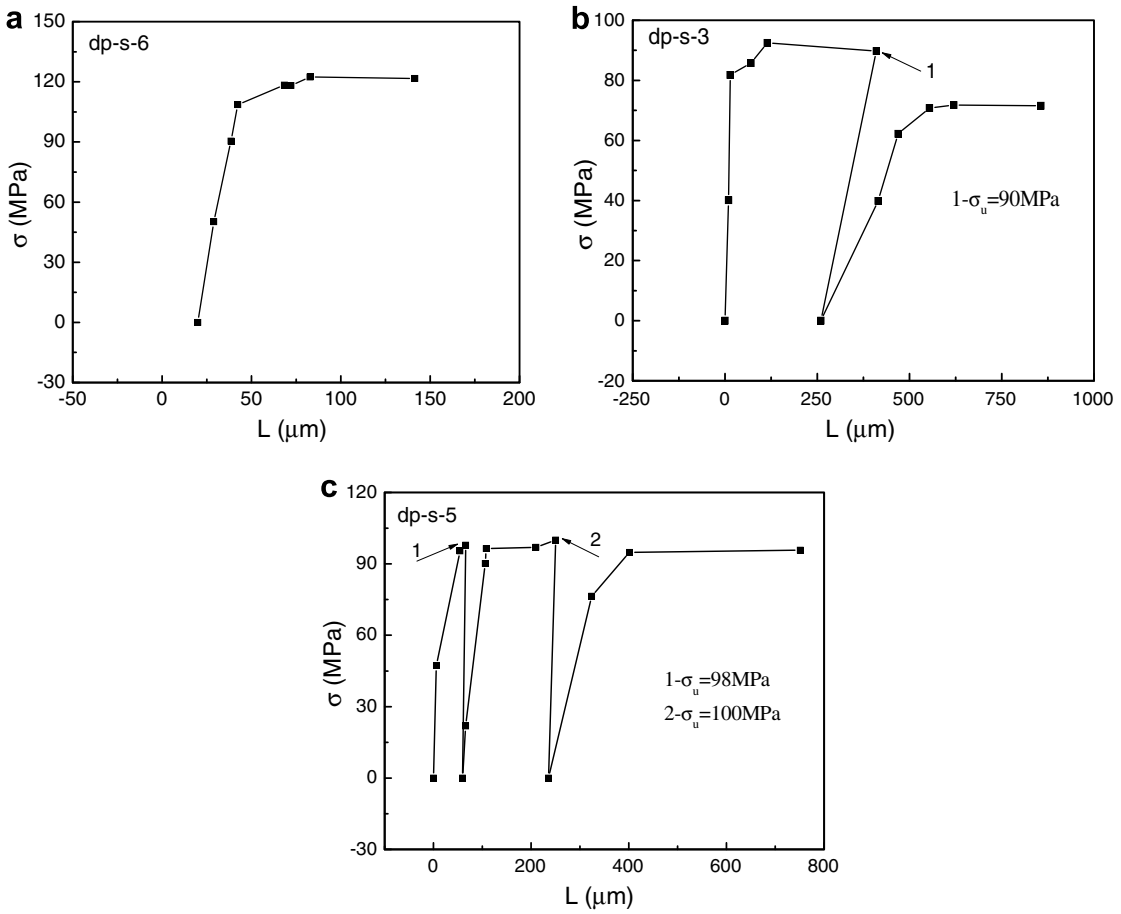

Fig. 4. Curves plotting applied stressσ against the lengths of main cracks L of duplex TiAl alloys (a) dp-s-6, (b) dp-s-3 and (c) dp-s-5. (Note: The applied stress,σ,is defined as the quotient of applied load divided by the original area of ligament of notched specimen.)

Table 3
Characteristic parameters of applied stresses and corresponding crack lengths measured in loading–unloading–reloading procedure

(a) Specimen fl-s-6													
σ (MPa)	0	92	0	91	145	0	126	150	155	147	0	68	74
L (μm)	0	30	0	25	58	50	110	245	352	952	952	1105	1114
(b) Specimen fl-s-10													
σ (MPa)	0	109	0	109	0	109	152	0	142	175	174	167	
L (μm)	0	126	66	134	63	223	711	685	748	1073	1832	1933	
(c) Specimen dp-s-3													
σ (MPa)	0		90		0		40		62		71		72
L (μm)	0		410		260		415		469		554		856

σ = applied stress, L = length of main crack propagation.

applied reload exceeded the preload. The facts, that crack opening was found to be fully reversible, provided that the main crack was produced at a load with the elastic regime.

(2) When preload was applied with the plastic regime such as 145 MPa for specimen fl-s-6 (Fig. 3c), after completely unloading, the main crack of 58 μm in length could not be fully closed. A remained crack of 50 μm in length was observed at the step of unload to zero. During the reloading process, the main crack was fully opened and extended further to a length of 110 μm at an applied reload of 126 MPa which was lower than the preload of 145 MPa. That is, the existing crack was extended at a value of the reload which was appreciably lower than that of the preload. This

phenomenon was observed for all specimens which were loaded-unloaded with the plastic regime. This phenomenon indicates the effect of damage resulting from the preloading–unloading process in this regime.

(3) After the preload reached a high level (as 155 MPa for specimen fl-s-6 (Fig. 3c)) 143 MPa for specimen fl-s-5 (Fig. 3b) and 90 MPa for specimen dp-s-3 (Fig. 4b), unstable extension of main cracks occurred. In subsequent unloading-reloading process, the main crack extended further and resulted in the final fracture at a reload, which was lower (specimens fl-s-9 and dp-s-5) or much lower (specimens fl-s-6, fl-s-5 and dp-s-3) than that of the preload.

In summary, the damage caused by the loading–unloading procedure was manifested in the extension of the main crack. The main crack not only decreased the ligament area, but also deteriorated the materials at the unloading step, which caused further extension of crack early at a lower reload.

3.2. Results and discussions of combined observations of the crack configurations and the fracture surfaces

Fig. 5a shows the configuration of the main crack 1 of specimen fl-s-6 at a preload of 92 MPa. The corresponding fracture surface is enclosed by Line 1 in Fig. 6. It was an interlamellar crack produced in elastic condition and did not penetrate the full thickness of specimen. Fig. 5b shows that the main crack was fully closed at the unloading step. Fig. 5c shows the reopening of the main crack at a reload of 91 MPa without further extension. In this case, the step of unloading has negligible effect on subsequent reloading process.

Fig. 7a shows the main crack configuration of fl-s-6 at a preload of 145 MPa. The crack length was 58 μm and the corresponding fracture surface was enclosed by Lines 2, 3 and 4 in Fig. 6. Fig. 7b shows that the crack was partly closed at the unloading step. Fig. 7c shows the reopening of the main crack at a reload of 126 MPa, which was lower than the preload

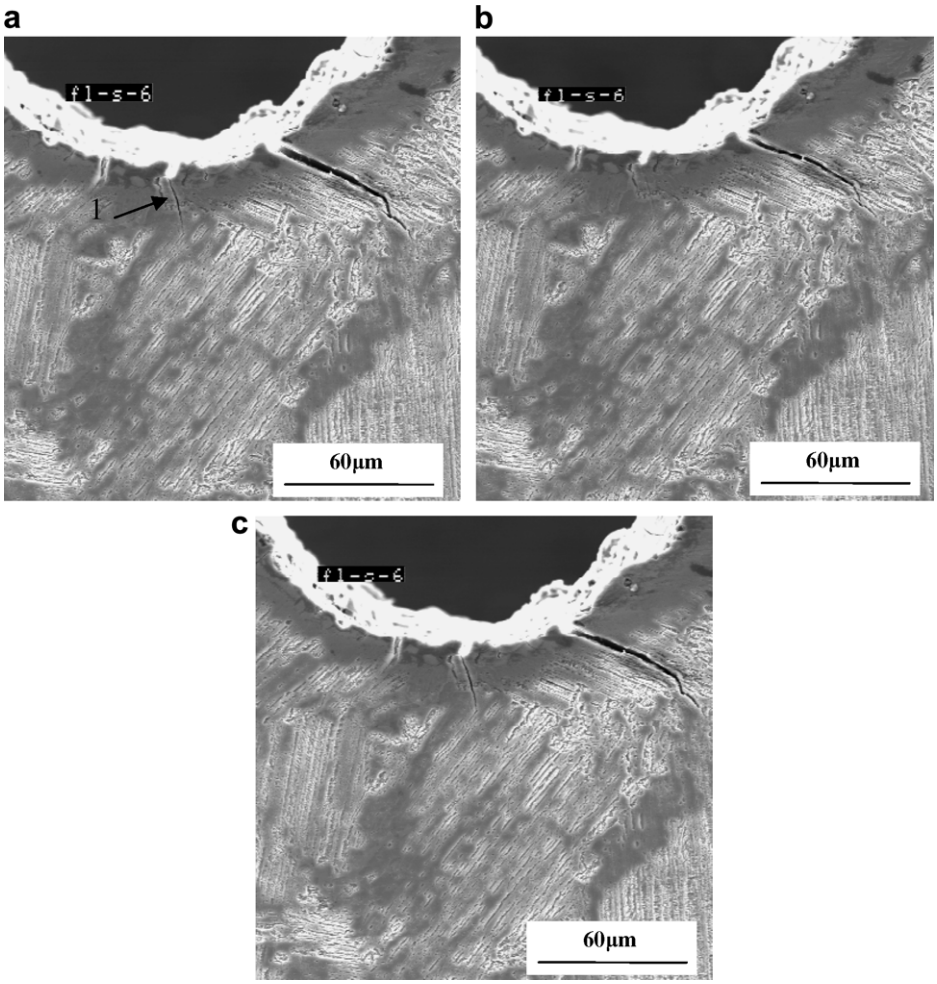

Fig. 5. Crack configuration of specimen fl-s-6 (a) at preload of 92 MPa, (b) completely unloading to 0 MPa and (c) at reload of 91 MPa.

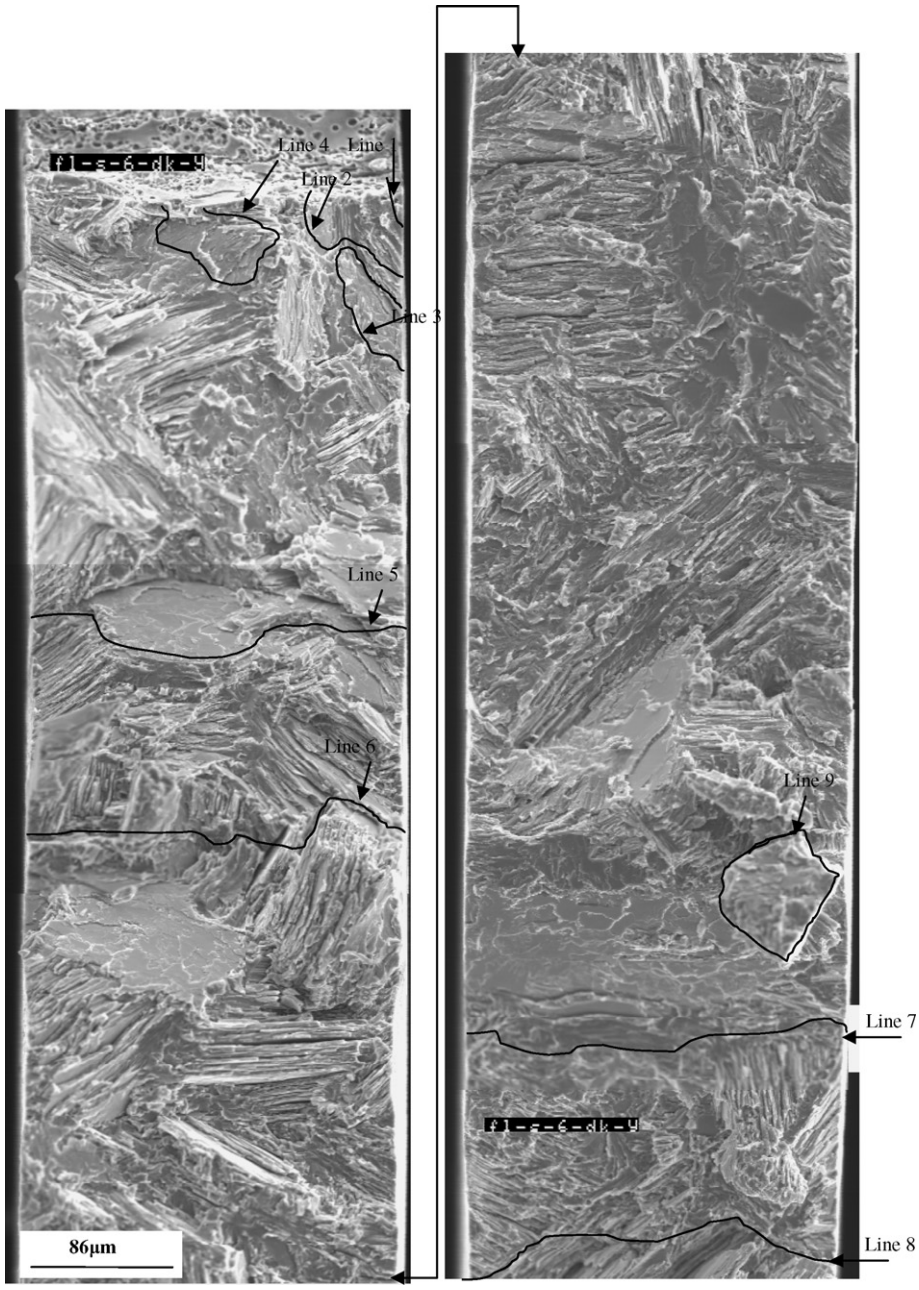

Fig. 6. Fracture surface of specimen fl-s-6.

of 145 MPa. The main crack extended further and connected to an interlamellar crack, which was produced in front of the main crack (in Fig. 7a) and fully closed in Fig. 7b. The reload of 126 MPa produced the total crack length of 110 μm, much longer than 58 μm produced by the preload of 145 MPa. It should be noted that this behavior was typical for all the samples investigated with loading–unloading procedure in the plastic region. When the load increased from 126 MPa to 155 MPa, the individual lamellar cracks connected and the main crack traversed the full thickness of specimen. The main crack with total length of 352 μm is shown in Fig. 8a, and the corresponding fracture surface is shown in Fig. 6 with Line 6 indicating the crack front. The reason, why an increment of 29 MPa (155–126 MPa) in applied load is related to the penetration of the crack through the full thickness, could be found in Ref. [12]. The increment of reload from 150 MPa to 155 MPa in Fig. 3c seemed to overcome a rugged area between Line 5 and Line 6 in Fig. 6 with dense trans-lamellar crack facets. Upon reloading at 155 MPa, an unstable extension of main crack from 352 μm to 952 μm broke out (Fig. 8b) which decreased the applied load to 147 MPa as shown in Fig. 3c. The corresponding fracture surface sectors, with Line 7 at its front (Fig. 6) show some large

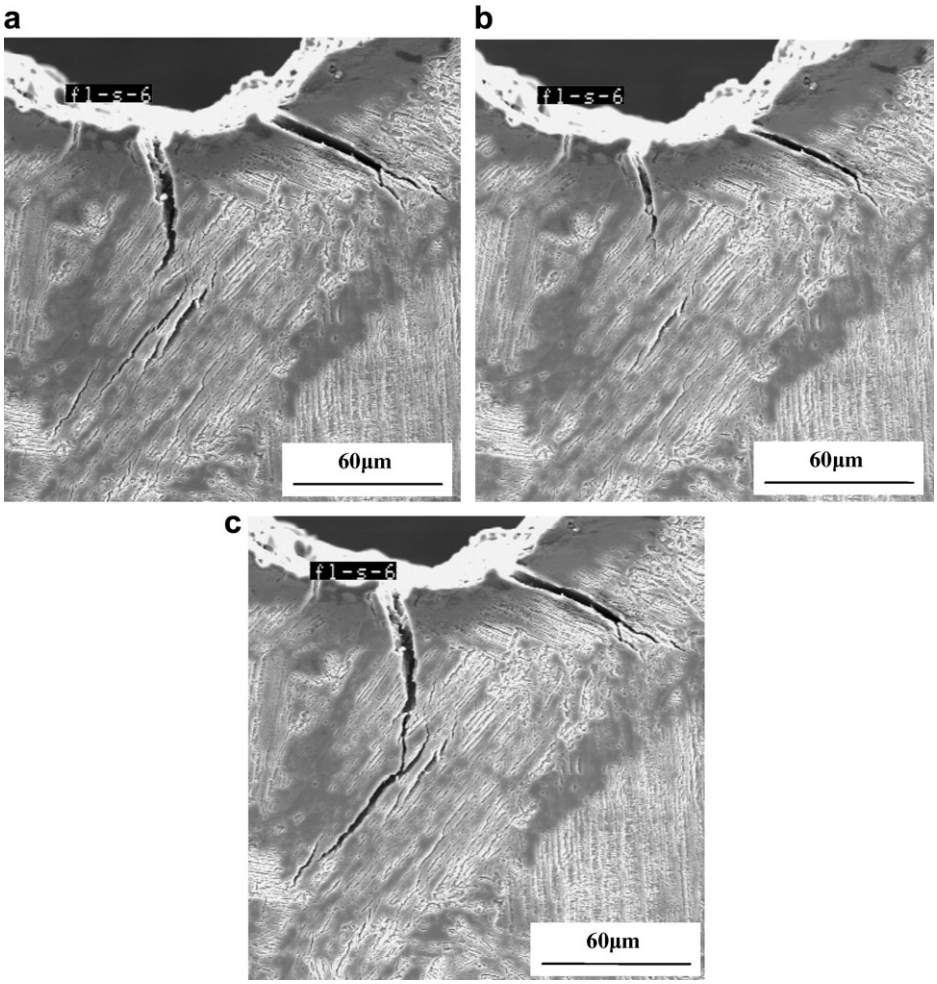

Fig. 7. Crack configuration of specimen fl-s-6 (a) at preload of 145 MPa, (b) completely unloading to 0 MPa and (c) at reload of 126 MPa.

interlamellar crack facets. The main crack is also seen just passing through an interlamellar cracking area and stopped in front of a rugged area with dense intra-lamellar crack facets (Line 7 in Fig. 6). This unstable extension is attributed to three factors: (1) elastic energy was accumulated during increasing the reload from 126 MPa to 155 MPa, (2) with extension of the main crack, the ligament area decreased and (3) the crack passed through a region with lamellae orientation which favored the interlamellar crack propagations. The crack stopped again in front of the region with lamellae oriented perpendicularly to the crack propagation after the accumulated energy was exhausted and the applied load was decreased. Fig. 8c shows the main crack configuration at the third step of unloading to zero (Fig. 3c). The width of the crack was appreciably narrowed in general, and the front sector was partly closed. Fig. 8d shows the crack configuration at reload of 68 MPa which was much lower than the preload 147 MPa. Compared with Fig. 8b, the width of the main crack was almost recovered and a microcrack of 153 μm in length was further extended at the tip. On the fracture surface this extension just covered the rugged area mentioned above (between Lines 7 and 8). At the same time by comparing Fig. 9a and b (magnified picture of Fig. 8c and d), a sector of the crack extended upward to tear an area bridging the main crack which is shown as a facet enclosed by Line 9 in Fig. 6 on fracture surface. Specimen fl-s-6 was fractured at an applied load of 74 MPa after an unstable extension as shown in Fig. 8e.

Fig. 10a shows the crack configuration of a DP specimen (dp-s-3) at a preload of 90 MPa, Fig. 10b shows the main crack configuration at the step of complete unloading to zero. Fig. 10c and d shows the crack configuration at reload of 62 MPa and 72 MPa which was much lower than the preload 90 MPa. Specimen dp-s-3 was fractured at an applied load of 71 MPa after an unstable extension. The effect of load–unload-induced damage produced by the preload 90 MPa in DP specimen (dp-s-3) was like that produced by preload of 150 MPa for a FL specimen fl-s-6 which was in the plastic regime. The main crack of 410 μm in length for specimen dp-s-3 could not be fully closed at the unload step. After completely unloading the sample, the crack length is 260 μm. In the reloading process, the main crack was fully opened and extended further to a length of

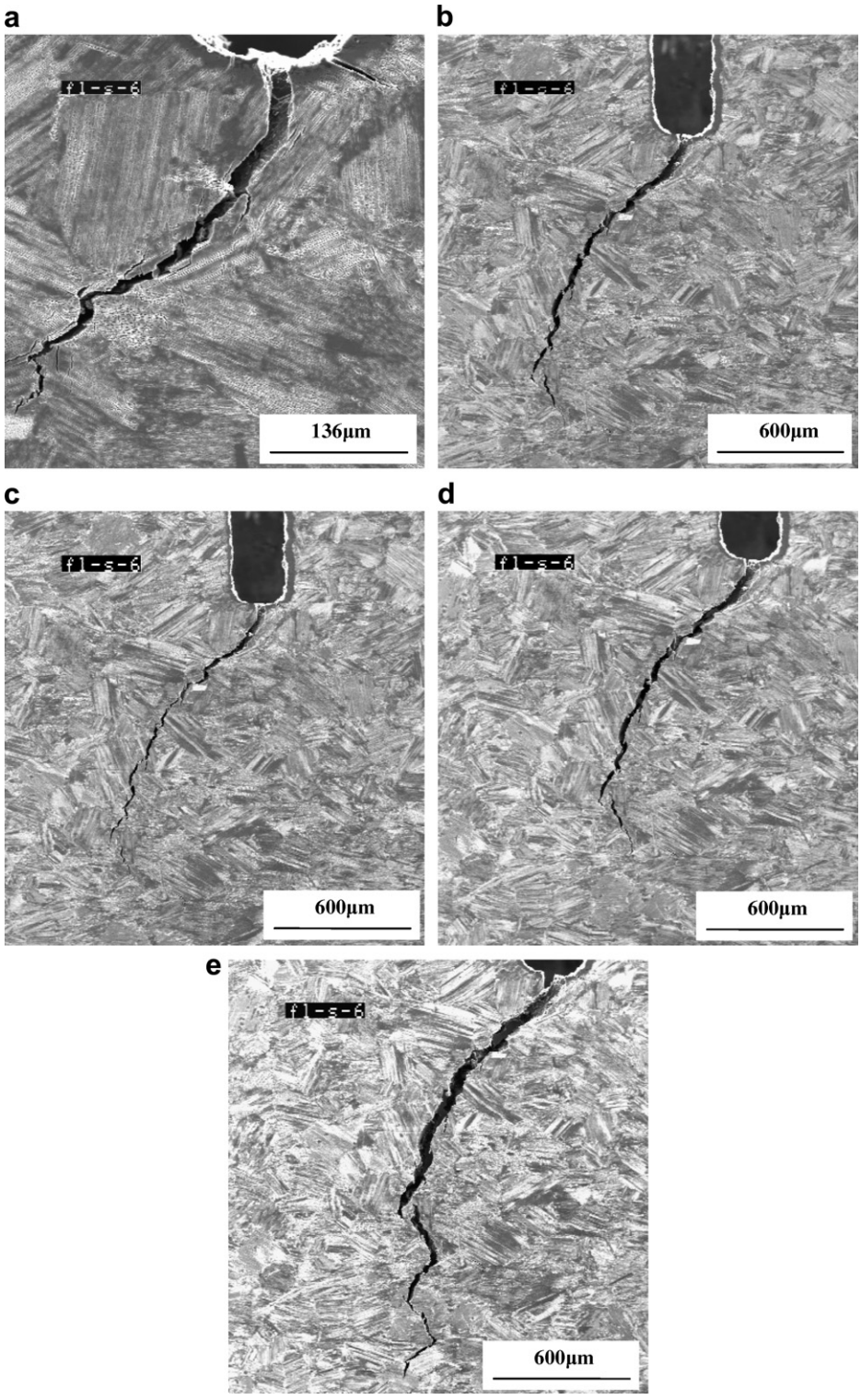

Fig. 8. Crack configuration of specimen fl-s-6 (a) at reload of 155 MPa, (b) after an unstable extension with decreasing the reload from 155 MPa to146 MPa, (c) completely unloading to 0 MPa, (d) at reload of 68 MPa and (e) at reload of 74 MPa.

415 μm at a 40 MPa of applied reload which was lower than the preload of 90 MPa. This phenomenon showed that the effect of preload–unload-induced damage occurred also for duplex microstructure specimens.

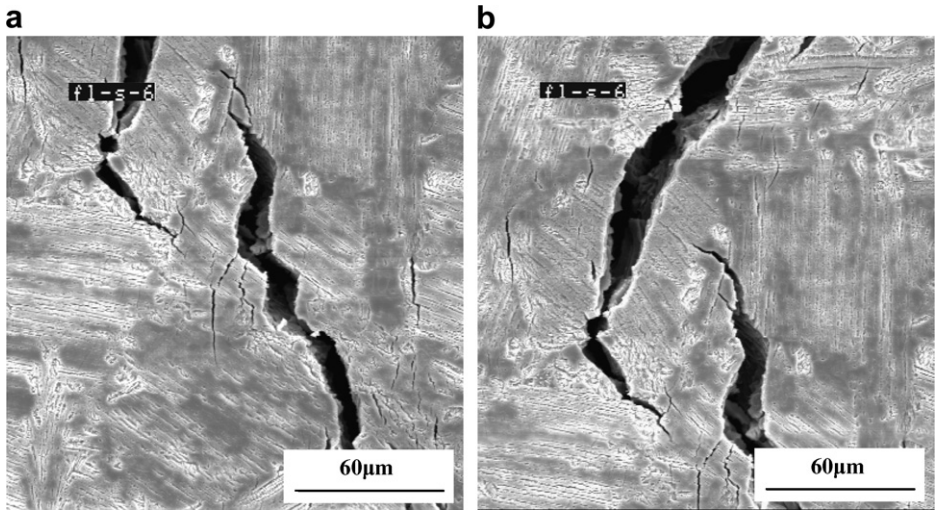

Fig. 9. Upward extension of crack sector after reloading (a) completely unloading to 0 MPa and (b) at reloading to 68 MPa.

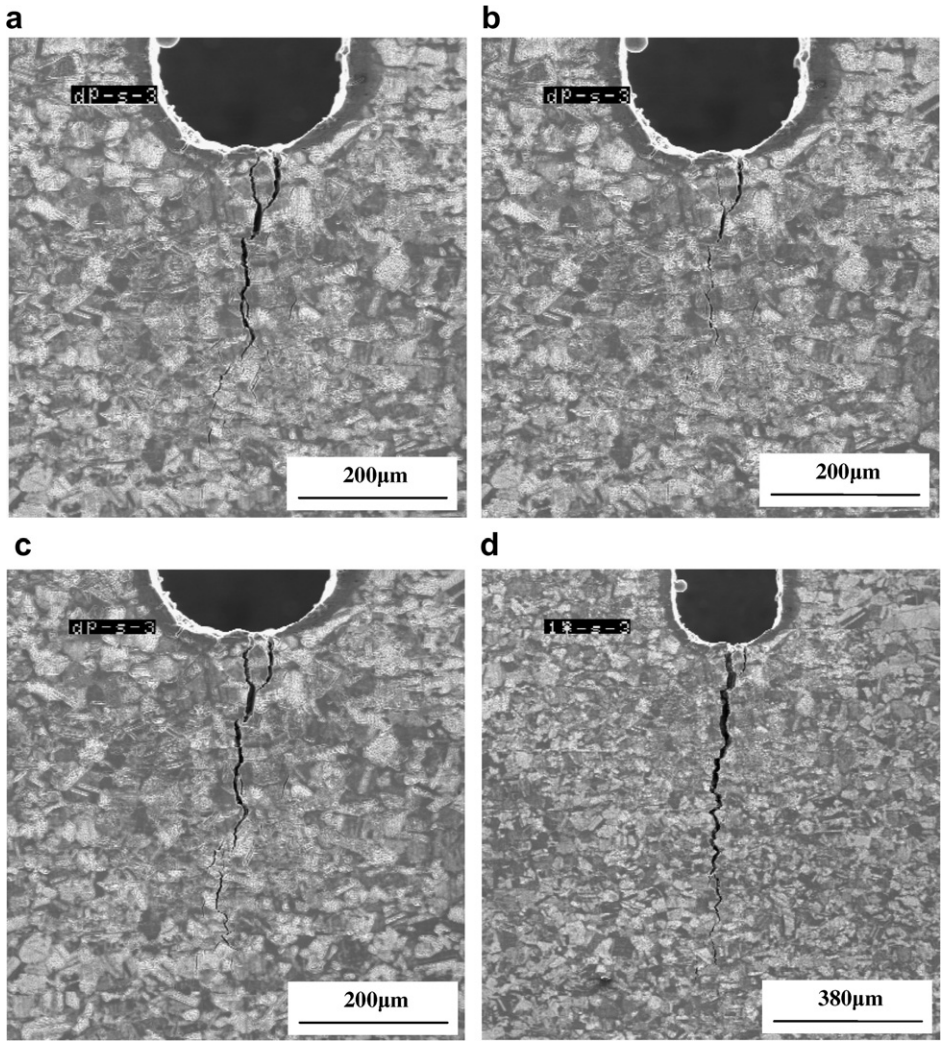

Fig. 10. Crack pattern during load–unload-reload process of specimen dp-s-3. (a) At preload of 90 MPa, (b) completely unloading to 0 MPa, (c) at reload of 62 MPa and (d) at reload of 72 MPa.

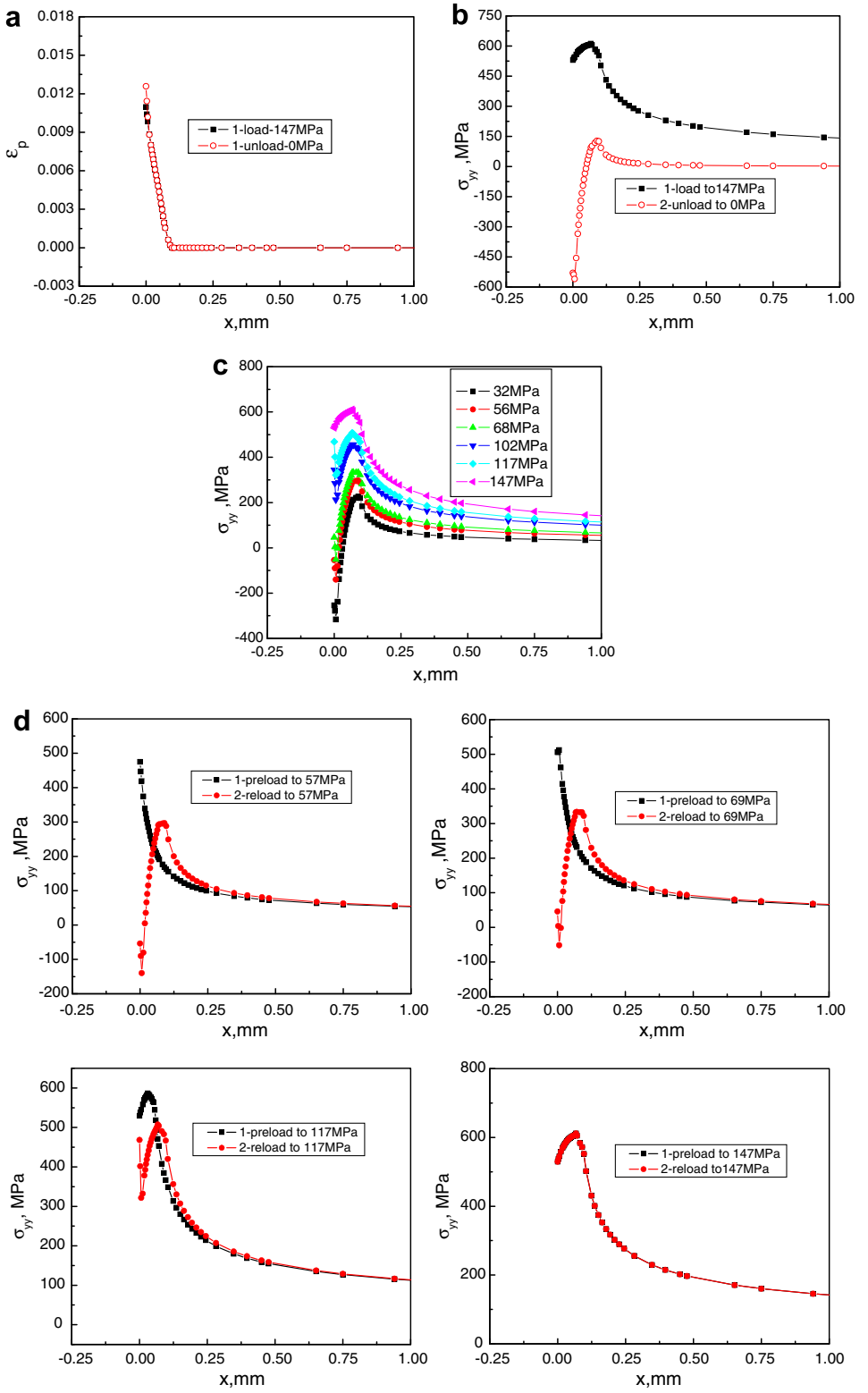

Fig. 11. Results of FEM calculations. (a) Distribution of plastic strain at preload of 147 MPa and unload. (b) Distribution of normal stress at preload of 147 MPa and unload. (c) Distribution of normal stress at various reloads with those at preload of 147 MPa and unload. (d) Comparison of distribution of normal stress at various preloads and reloads.

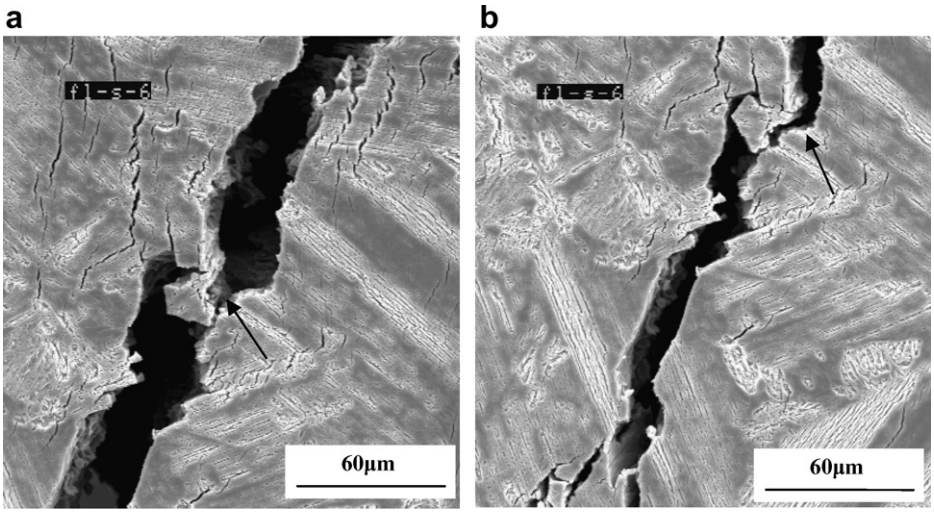

Fig. 12. Crack extends while it is closing in the process of unloading (a and b) specimen fl-s-6. (a) At preload of 147 MPa and (b) completely unloading to 0 MPa.

3.3. Results and discussions of FEM calculation

Fig. 11 shows the distributions of plastic strain ε_p (a) and normal stress σ_{yy} (b) at the preload of 147 MPa and after completely unloading to zero of specimen fl-s-6. Fig. 11c shows the distributions of σ_{yy} at a series of successively increasing reloading values in addition to the two curves in Fig. 11b. In Fig. 11d the distributions of normal stress at reload overlaps on that at preload. Although these calculation results only qualitatively evaluate the variation of stress and strain distribution during loading–unloading–reloading processes, following ideas can be drawn: (1) In front of the main crack tip a plastic zone was formed, which extended to about 125 μm and caused the stress intensification. After completely unloading to zero, a compressive stress region developed within 50 μm and ahead of the region the tensile stress remained in a region around 200 μm in length. Due to the residual tensile stress, during the reloading process the normal stress σ_{yy} was developing faster than that in preload process as shown in Fig. 11d. However, the peak values of σ_{yy} developed at various reload levels never exceeded those of σ_{yy} produced by the preload of 147 MPa. These results mean that the further extension of the main crack at lower values of reloads was not caused by a higher normal stress induced by the residual tensile stress. Therefore, the further extension of the main crack at a lower reload should be attributed to the deterioration of material at the crack tip produced in unloading process. In recent work [13], the authors found that the compressive stress beyond 600 MPa could cause serious damage of TiAl alloys. As shown in Fig. 11b, due to the retained plastic strain at the crack tip, a compressive stress around 600 MPa can be produced in the unloading process. This maybe the reason of the damage produced. Fig. 12 shows an extension of a crack sector while the total crack was closed during unloading process. This may indicate that at the tip region further damage of material occurred in the unloading process. However, the exact mechanism, which can illustrate the physical process in the resident plastic region at the crack tip for TiAl alloy will be investigated in future work by new concept such as cohesion strength of low index cleavage planes in gamma TiAl alloy [14].

3.4. Effects of microcracks

As mentioned in introduction the fracture behavior in a notched TiAl specimen is different from that in a smooth tensile test specimen. In a smooth tensile test specimen, the fracture occurs at the weakest cross section where the density of microcracks is highest. Therefore, the microcracks produced during the preloading process are expected to decisively reduce the final fracture stress. However, in a notched specimen the main crack propagation is confined to a narrow strip extending in front of the notch. The main crack extends along a path where a high tensile stress is coupled with a low fracture resistance. The latter is consistent with lamellae's orientation which favors to interlamellar cracking. As shown in Fig. 13, there are many translamellar microcracks present between the two sectors of the main crack. Nevertheless, the main crack extends bypasses these microcracks and follows an interlamellar path. In this case, the effect of microcrack is minor. This observation was typical for all the notched samples.

3.5. Two Special issues

3.5.1. Mechanism of high resistance to crack propagation

From Fig. 3f, it is found that the specimen fl-s-10 shows the highest fracture stress and the longest crack extension before final fracture. The mechanisms behind this finding will now be discussed. In Fig. 3f there are four values on the ascendant

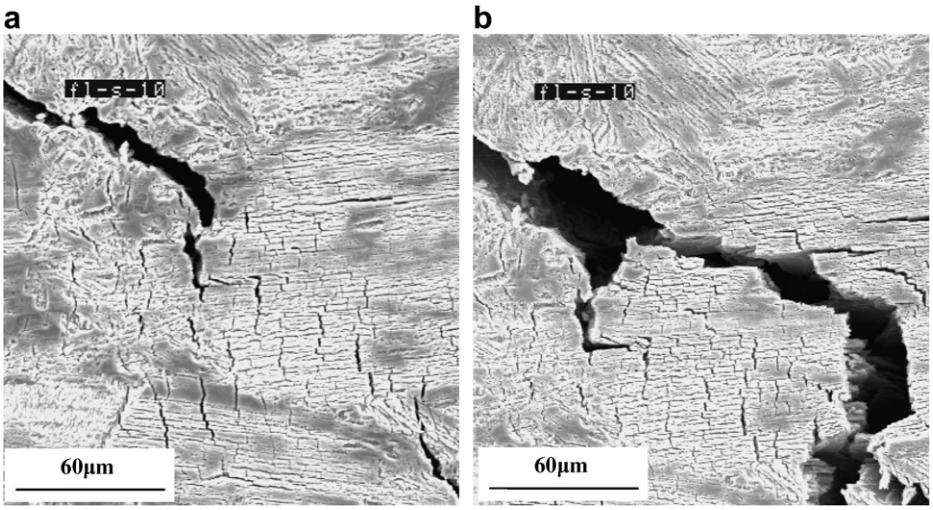

Fig. 13. Main crack bypasses a lot of microcracks in specimen fl-s-10. (a) At reload of 171 MPa and (b) at reload of 169 MPa.

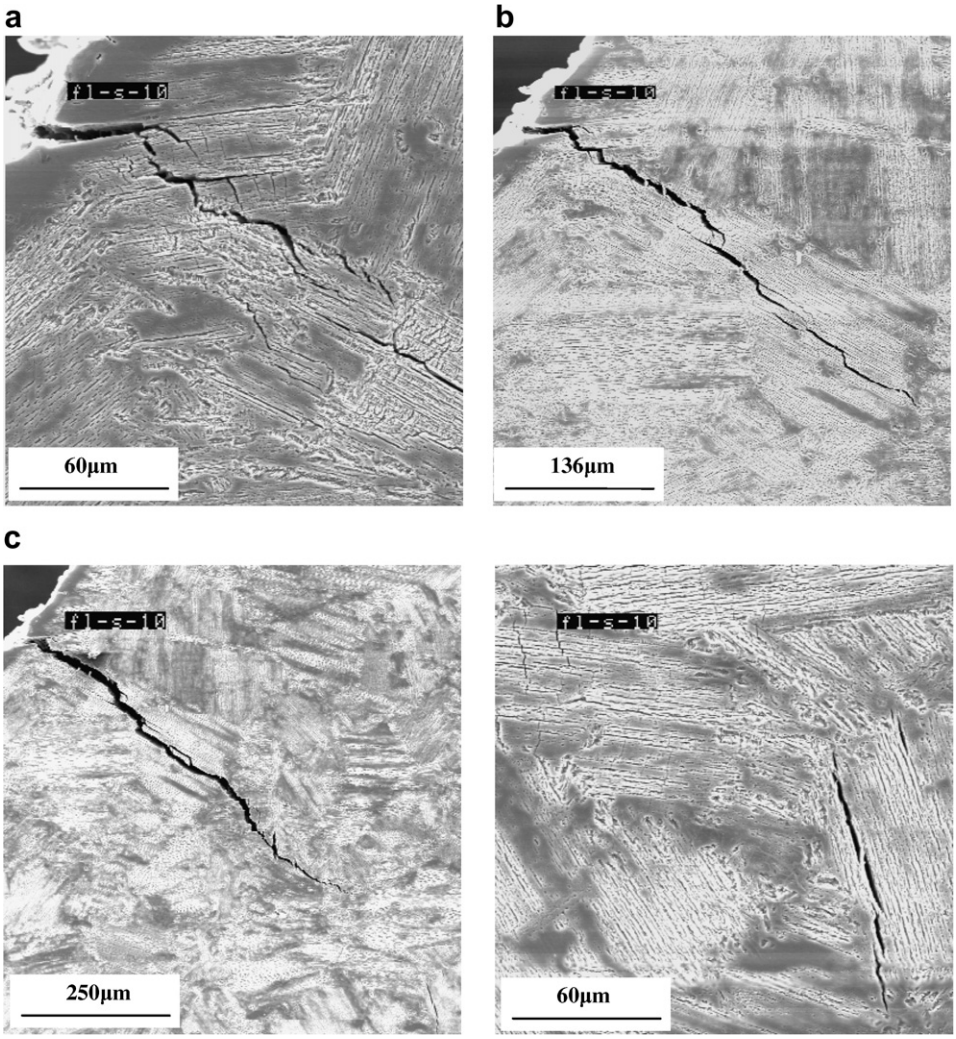

Fig. 14. Crack configurations of specimen fl-s-10 at applied stresses (a) 107 MPa, (b) 123 MPa, (c) 152 MPa and (d) the successive crack propagation configurations developed during the applied stress increased from 174 MPa to 175 MPa.

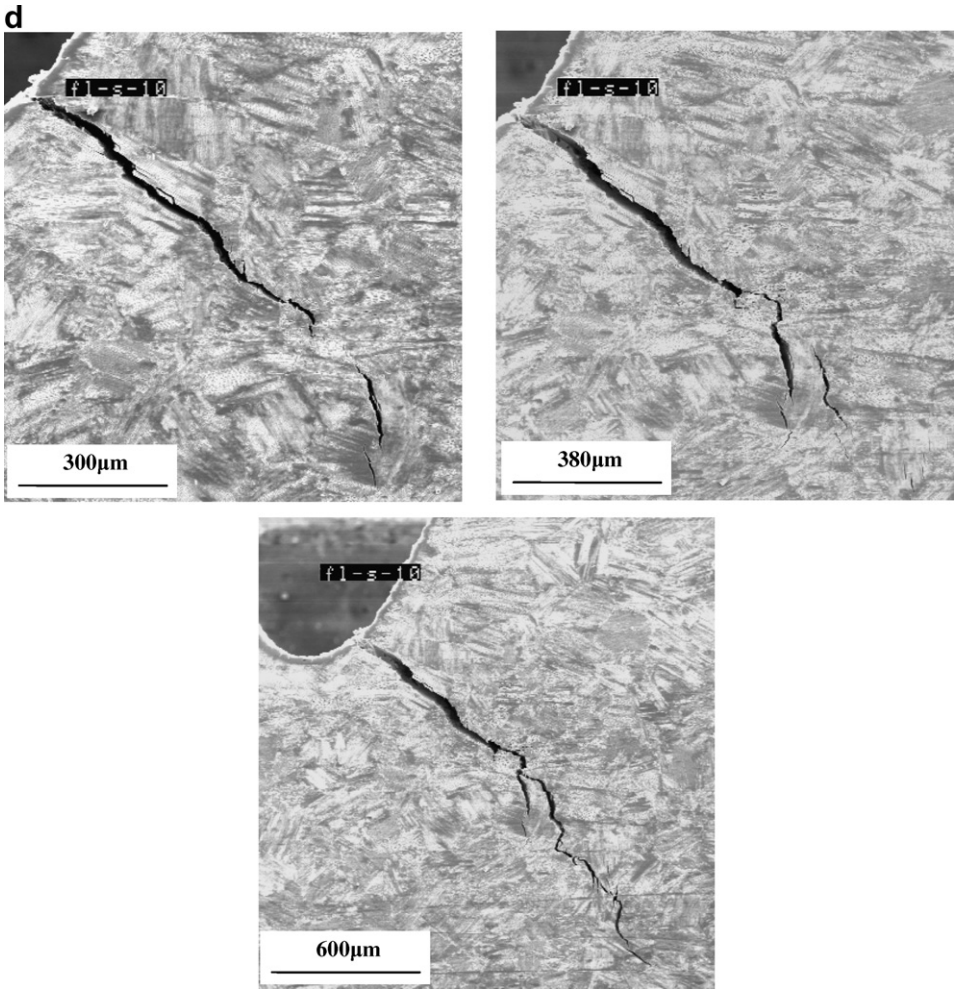

Fig. 14 (*continued*)

stress locus curve, i.e., 109 MPa, 123 MPa, 152 MPa, and 175 MPa, which characterize the four steps of increment in applied stress. Fig. 14 shows the crack configurations at these applied stresses. Fig. 15 shows the corresponding fracture surface sector. For the first step from 0 to 109 MPa, the crack extended to 126 μm in length (true crack length) shown in Fig. 14a. During this process a large interlamellar crack with a small area of translamellar crack on the left was produced, which is shown by the area enclosed by Line 1 in Fig. 15. After four steps of unloadings and reloadings, the applied stress enhanced to 123 MPa, and the main crack extended to 224 μm as shown in Fig. 14b. On the fracture surface, the increment of crack covered an area (enclosed by Line2) mixed with inter- and translamellar cracking. The rugged part on the right top corner was considered to be cracked at this step, because an unstable crack extension followed this step. It means that the crack had penetrated through the full thickness of specimen (Ref. [12]). For the next step, the stress was enhanced by 123–152 MPa, which extends the crack through a large rugged area enclosed by Line 3 in Fig. 15. The crack extension is shown in Fig. 14c, which covers about 200 μm translamellar region. At this step, some interlamellar cracks were produced a distance ahead of the main crack as shown at the right bottom corner of Fig. 14c and a close view is shown in the right-hand Figure. At the last step, stress was enhanced to 175 MPa. The 23 MPa enhancement was demanded to turn the main crack from a direction about 45° inclined to the central axis to parallel to it. The process is shown in three pictures of Fig. 14d. On fracture surface the main crack cuts through a dense translamellar region enclosed by Line 4. At the first glance, it seems that the resistance to crack extension results from tearing the ligament bridge between the main crack and the existing interlamellar crack. However, from the Fig. 14d, it is revealed that a new crack was produced and through it the main crack turned its direction from 45 degree declined to perpendicular to the maximum tensile stress. In general, for specimen fl-s-10, the resistance presented at each step was produced by extending the main crack through a translamellar region for adjusting the main crack direction from an inclined orientation to the straight one. However, due to the inclined orientation of the lamellae, cracks preferred to extend along with their interfaces, which deflected the main crack away from the path with the highest stress. With the extension of the crack in an inclined orientation, the distances of the crack tip from both the notch root and from the central axis

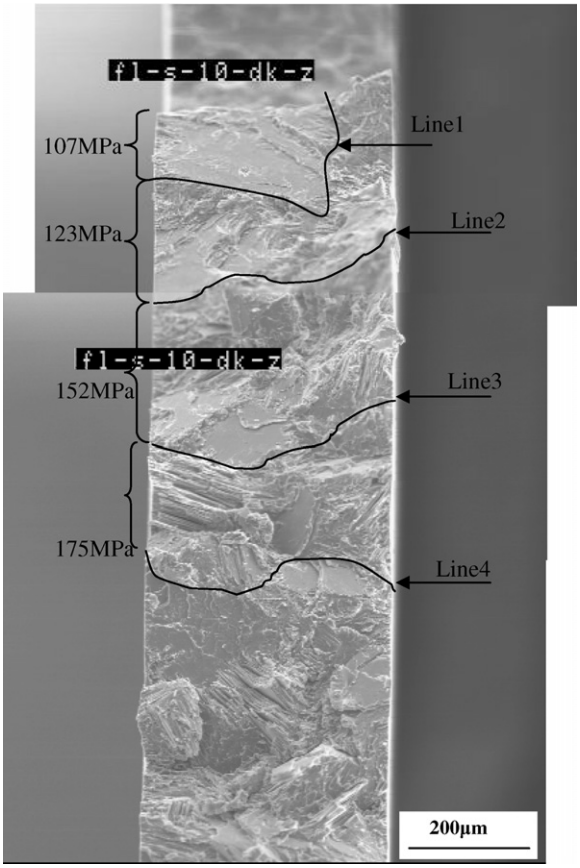

Fig. 15. Fracture surface of specimen fl-s-10.

increased. In this case, the applied stress should be increased for further extending crack through regions even with same resistance. Deviation of the main crack by lamellae with inclined orientation was found as the main mechanism of toughening in a fully lamellar TiAl alloy. This function is just like the one observed in composite materials.

Except for the highest resistance presented in specimen fl-s-10, the three loading–unloading processes showed appreciable, but not remarkable, effects on the further extension of the main crack. The weak effects of the loading–unloading process on the damage is also attributed to the inclined crack, the residual plastic region at its tip was subjected to a weaker effect of the elastic stress produced in the unloading step.

3.5.2. Weaker crack-resistance of DP alloy in notched specimens

By comparing Figs. 3 and 4, it is found that the fracture stresses of DP specimens are lower than that of FL specimens. Fig. 16 shows the fracture surfaces of specimens fl-s-10 and dp-s-3. By comparison of these Figures, the reason why the DP specimens show a lower crack-resistance can be summarized as follows:

(a) Even though DP specimens show much finer crack facets, the FL specimens show much more rugged surfaces in general. Even on the facets looking as translamellar cracking, the roughness is much lower in DP specimens than the roughness in FL specimens. The impression is that the lamellae are finer and that the orientation differences between lamellae are less for DP specimen than for FL specimens.

(b) The angles with which the fracture facets inclined with each other are much more distinct and much larger for FL specimens (as shown by facets on the right top corner of Fig. 16b and the middle of Fig. 16a) than for DP specimens. These results were apparently caused by the large grains with various orientation-inclined lamellae in FL specimens. This is considered as the reason why the coarse grain TiAl alloy shows higher fracture toughness.

(c) By comparing of Figs. 10, 14, 15, it is apparent in a notched specimen, the path of crack extension is much straighter in DP specimen than the path in FL specimen. In the DP specimen, the crack is constrained in the narrow strip of high stress. This also attributes to the low fracture toughness of DP specimen.

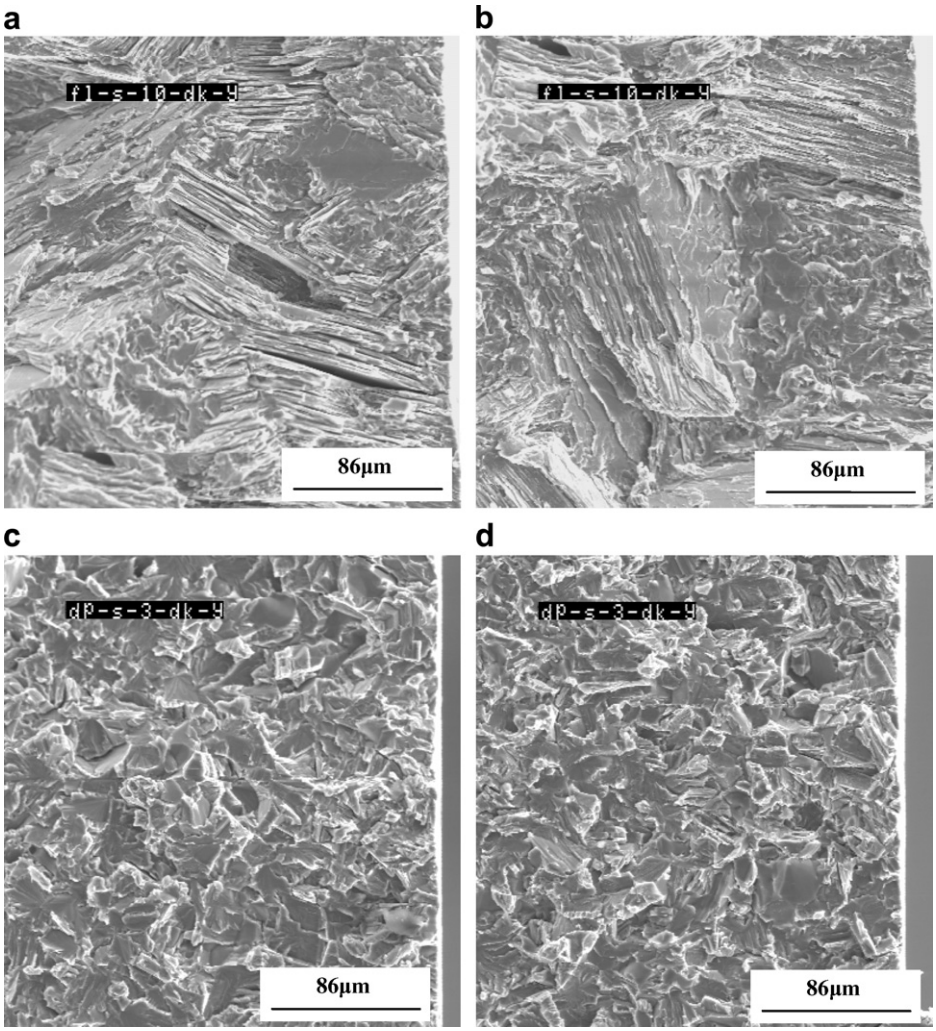

Fig. 16. Fracture surfaces of specimen (a and b) fl-s-10, (c and d) specimen dp-s-3.

4. Conclusions

Based on in situ observations and analysis of crack configurations and fracture surfaces of notched specimens of TiAl alloys, effects of loading–unloading induced damage on the fracture behavior are summarized as follows:

(a) At an elastic regime, a loading–unloading process has no effect on the fracture behavior in subsequent reloading process.
(b) At a plastic regime, even at a value of the reload much lower than that of preload, the reload further extends the existing crack; and after a heavy loading–unloading process, the crack extends and results in the fracture at a reload value which is lower than that of the preload.
(c) Microcracks produced in the processes of loading–unloading have minor effects on the resistance to crack propagated in a notched specimens.
(d) Lower resistance of DP microstructure results from its fine grain with small orientation differences between lamellae.

Acknowledgements

This work was financially supported by the National Nature Science Foundation of China (No. 50471109) and Nature Science Foundation of Gansu Province (No. 3ZS061-A25-037) and Opening Foundation of State Key Laboratory of Gansu Advanced Non-ferrous Metal Materials. Authors express their sincere gratitude to Mrs. Ello for her help in language edition.

References

[1] Chan KS, Kim Y-W. Influence of microstructure on cracktip micromechanics and fracture behaviors of a two-phase TiAl alloy. Metall Trans 1992;23A(6):1663–77.
[2] Lu YH, Zhang YG, Qiao LJ. The fracture mechanism of a fully lamellar γ-TiAl alloy through in situ SEM observation. Intermetallics 2000;12(8):1443–5.
[3] Chan KS, Onstott J, Kumar KS. The fracture resistance of a binary TiAl alloy. Metall Materal Trans 2000;31A(2):71–80.
[4] Yokoshima S, Yamaguchi M. Fracture behavior and toughness of PST crystals of TiAl. Acta Mater 1996;44(3):873–83.
[5] Inui H, Oh MH, Nakamura A, Yamaguchi M. Room-temperature tensile deformation of polysynthetically twinned (PST) crystals of TiAl. Acta Metall Mater 1992;40(11):3095–104.
[6] Arata JJM, Kumar KS, Curtin WA, et al. Crack growth in lamellar titanium aluminide. Int J Fract 2001;111(2):163–89.
[7] Zheng RT, Zhang YG, Chen CQ. Microcrack nucleation and its effect on the plastic deformation of FL γ-TiAl alloy. J Mater Sci 2004;39:1721–5.
[8] Bartels A, Clemens H, Dehm G. Strain rate dependence of the deformation mechanisms in a fully lamellar γ-TiAl-based alloy. Z Metallkd 2002;92(3):180–5.
[9] Zhou Y, Xia Y. Tensile mechanical behavior of TiAl (FL) at high strain rate. J Mater Sci 2000;34:925–9.
[10] Cao R, Zhu H, Chen JH, et al. Effects of microcrack-damage on fracture behavior of TiAl alloy part I displacement-controlled tensile test. Mater Sci Eng 2008;474:1–14.
[11] Cao R, Zhu H, Chen JH, et al. Effects of microcrack-damage on fracture behavior of TiAl alloy. Part II: load-controlled tensile test. J Mater Sci 2008;43:299–311.
[12] Cao R, Yao HJ, Chen JH, et al. On the mechanism of crack propagation resistance of fully lamellar TiAl Alloy. Mater Sci Eng 2006;420A(1–2):122–34.
[13] Cao R, Lin YZ, Hu D, Chen JH. Fracture behaviors of a TiAl alloy under various loading modes, Eng Fract Mech; 2008, in press. doi:10.1016/j.engfracmech.2008.01.013.
[14] Yoo MH, Yoshimi K. An empirical model for ideal work of adhesion: transition-metal aluminides and silicides. Intermetallics 2000;8:1215–24.